J. Chem. Sci., Vol. 123, No. 1, January 2011, pp. 5–13. © Indian Academy of Sciences.

Synthesis, structure and ionic conductivity in scheelite type $Li_{0·5}Ce_{0·5-x}Ln_xMoO_4$ (x = 0 and 0·25, Ln = Pr, Sm)

DIPANKAR SAHA[a], GIRIDHAR MADRAS[a,b], ANINDA J BHATTACHARYYA[a] and TAYUR N GURU ROW[a,*]

[a]Solid State and Structural Chemistry Unit, Indian Institute of Science, Bangalore 560 012, India

[b]Department of Chemical Engineering, Indian Institute of Science, Bangalore 560 012, India
e-mail: ssctng@sscu.iisc.ernet.in

MS received 25 August 2010; revised 5 December 2010; accepted 6 December 2010

Abstract. Scheelite type solid electrolytes, $Li_{0·5}Ce_{0·5-x}Ln_xMoO_4$ (x = 0 and 0·25, Ln = Pr, Sm) have been synthesized using a solid state method. Their structure and ionic conductivity (σ) were obtained by single crystal X-ray diffraction and ac-impedance spectroscopy, respectively. X-ray diffraction studies reveal a space group of $I4_1/a$ for $Li_{0·5}Ce_{0·5-x}Ln_xMoO_4$ (x = 0 and 0·25, Ln = Pr, Sm) scheelite compounds. The unsubstituted $Li_{0·5}Ce_{0·5}MoO_4$ showed lithium ion conductivity ~10^{-5}–10^{-3} $\Omega^{-1}cm^{-1}$ in the temperature range of 300–700°C ($\sigma = 2.5\times10^{-3}$ $\Omega^{-1}cm^{-1}$ at 700°C). The substituted compounds show lower conductivity compared to the unsubstituted compound, with the magnitude of ionic conductivity being two (in the high temperature regime) to one order (in the low temperature regime) lower than the unsubstituted compound. Since these scheelite type structures show significant conductivity, the series of compounds could serve in high temperature lithium battery operations.

Keywords. Scheelite; ionic conductivity; ac-impedance spectroscopy.

1. Introduction

Development of solid electrolytes with fast lithium ion transport is one of the key areas of current research for the development of all solid state lithium (ion) batteries in portable electronics, medicine and space applications.[1,2] Solid electrolytes possess several advantages compared to organic liquid electrolytes used in commercial batteries. The advantages are essentially with regard to safety issues such as leakage, corrosion, inflammability. In addition, depending on the type of chemical constituents and their concentration, solid electrolytes have sometimes exhibited ionic conductivity and electrochemical stability at par with or even better than commercial liquid electrolytes. Moreover, solid inorganic electrolytes are stable under high voltage as well as at higher current. The latter is essential, as there is a lot of demand for high power (high current) density batteries. Additionally, as solid electrolytes possess far superior mechanical properties compared to liquid electrolytes, there exist larger possibilities for synthesis of solid electrolytes in varied morphologies leading to battery performances (high volumetric and gravimetric capacities, long shelf life) requisite for commercial applications.

The quest for high lithium ion conductivity in wide range of inorganic metal oxides with different crystallographic structures has been a major area of research over past few decades as discussed in several reviews.[1,3,4] Some of the important examples where high ionic conductivity (~10^{-4}–$10^{-3}\Omega^{-1}cm^{-1}$) have been observed are: (a) perovskite type lithium lanthanum titanate $Li_{3x}La_{(2/3)-x\square(1/3)-2x}TiO_3$($0 < x > 0·16$; □ denotes vacancy)[5–9], (b) doped NASICON type lithium compounds $LiTi_2(PO_4)_3$ (Ti substitution by Al, Cr, Ga, Fe, Sc, In, Lu, Y, or La)[10,11], (c) thio-LISICON family of compounds (Li_2S – GeS_2, Li_2S – GeS_2 – ZnS and Li_2S – GeS_2 – Ga_2S_3) $Li_{4+x-\delta}Ge_{1-x+\delta}Ga_xS_4$[12,13] and (d) garnet-type compound such as $Li_5La_3M_2O_{12}$ (M = Ta, Nb)[14] $Li_6La_2BaTa_2O_{12}$.[15,16] Scheelite type lithium ion conductors have also attracted interest particularly for lithium battery operation at high temperature (300–600)°C.[17] It has been reported that substituted scheelite $A_{1-x}Li_{2x}BO_4$ (A = Ca, Sr, Ba and B = W, Mo) shows

*For correspondence

liquid-like ionic conductivity ~(10^{-2}–10^{-1}) $\Omega^{-1}cm^{-1}$ in the temperature range of 700–900°C. $LiLnMo_2O_8$ also belongs to the category of scheelite structures.[18] These compounds are potential candidates for inorganic pigment[19] and laser wave guide material.[20]

In this article, we report the synthesis, structure and ionic conductivity of scheelite type $Li_{0.5}Ce_{0.5-x}Ln_xMoO_4$ (x = 0 and 0·25, Ln = Pr, Sm). The compounds reported are $Li_{0.5}Ce_{0.5}MoO_4$, $Li_{0.5}Ce_{0.25}Pr_{0.25}MoO_4$ and $Li_{0.5}Ce_{0.25}Sm_{0.25}MoO_4$, hereafter, referred to as LCM, LCPM and LCSM, respectively.

2. Experimental

2.1 *Materials*

Reagent grade powder of CeO_2, Pr_6O_{11}, Sm_2O_3 (99·9%, Sigma Aldrich), MoO_3 (99·0% SD Fine Chemical, India) and Li_2CO_3 (99·0% S D Fine Chemical limited, India) were used as starting materials.

2.2 *Synthesis*

$Li_{0.5}Ce_{0.5-x}Ln_xMoO_4$ (x = 0 and 0·25, Ln = Pr, Sm) were prepared by solid state method. The appropriate molar ratios of these compounds were mixed and ground well with an agate pestle and mortar and cast into pellets and fired at 700°C for 24 h. Resulting pellets were reground and again annealed for 24 h at 700°C to obtain pure phase.

2.3 *Phase characterization of LCM, LCPM and LCSM*

Differential scanning caloriemetry (DSC) measurements were carried out (Mettler Toledo STAR^e) at a heating rate of 10°C min^{-1} under N_2 atmosphere in the temperature range of 25–550°C. The crystallographic phases were identified by powder X-ray diffraction (Philips, X'pert Pro powder diffractometer with X'celerator detector). The x-ray powder data were collected from 5 to 90° in 2θ with a step size of 0.017 with data collection time per step being 90 seconds. Single crystals of each material were grown by melt-cool technique. The compounds were melted at 1050°C in a platinum crucible and cooled at a controlled rate of 25°C h^{-1}. This yielded orange-red block type crystals and a suitable crystal for single crystal X-ray data collection was selected using a polarising microscope. Single-crystal X-ray diffraction data for LCM were collected on a Bruker AXS SMART APEX CCD diffractometer. The X-ray generator was operated at 50 kV and 35 mA using Mo-Kα radiation (λ = 0·71073 Å). Data were collected with ω scan width of 0·3°. A total of 606 frames were collected in four different settings of ϕ (0°, 90°, 180°, 270°) keeping the sample to detector distance fixed at 6·03 cm and the 2θ value fixed at −25°. The data were reduced using SAINTPLUS and an empirical absorption correction was applied using the package SADABS.[21] The remaining crystals were collected on Xcalibur™ Mova E diffractometer with four circle kappa goniometer and Eos CCD detector in *CrysAlis CCD, Oxford Diffraction* with X-ray generator 50 kV and 1 mA, using MoK_α radiation (λ = 0·7107 Å). The cell refinement and data reduction were accomplished using *CrysAlis*

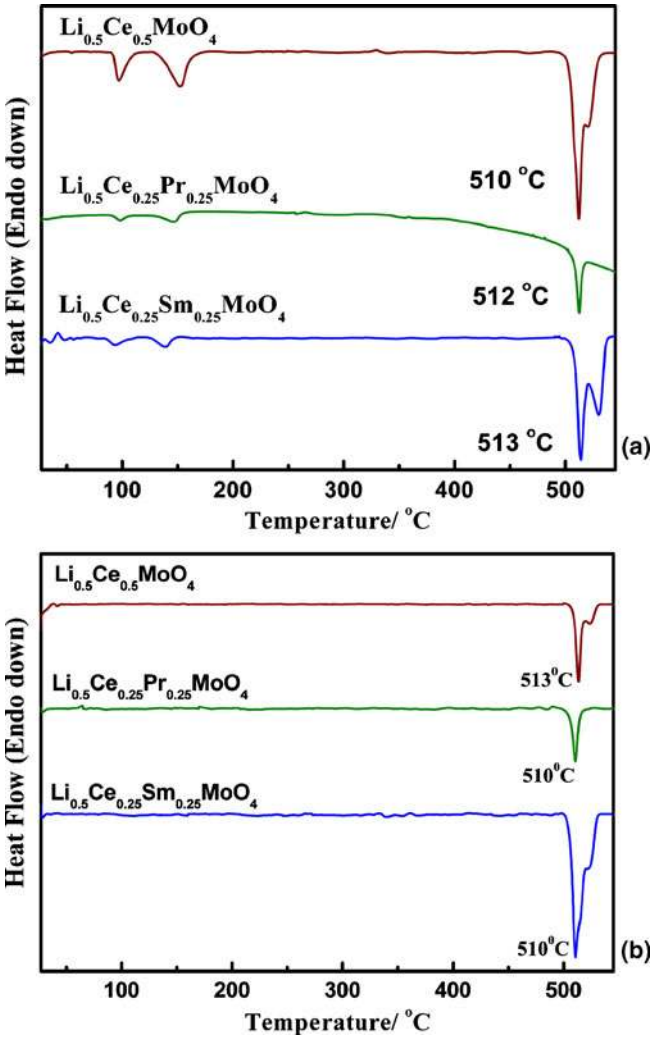

Figure 1. Differential scanning caloriemetry for LCM, LCPM and LCSM: as (**a**) synthesized samples. (**b**) Preheated samples (120°C/ 12 h; vacuum); heat/cool rate of 10°C min^{-1} under N_2 atmosphere.

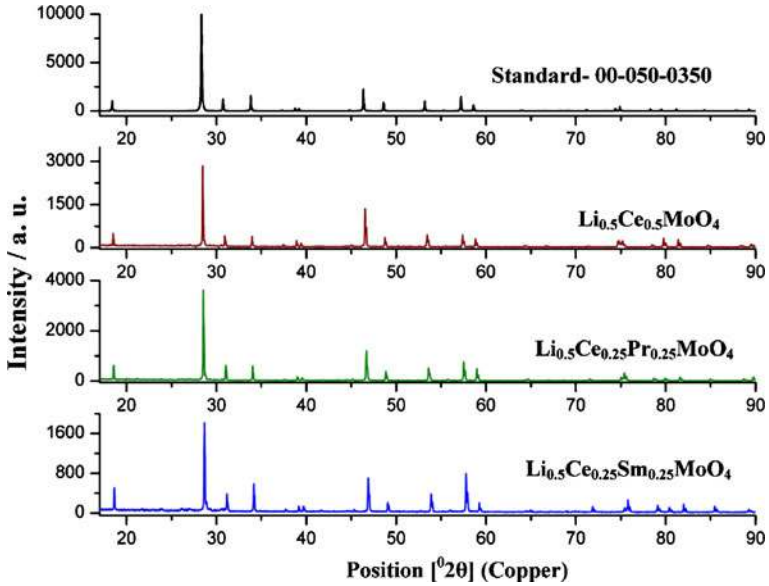

Figure 2. Powder X-ray diffraction pattern of synthesized $Li_{0·5}Ce_{0·5-x}Ln_xMoO_4$ (x = 0 and 0·25, Ln = Pr, Sm) at room temperature (= 25°C) in comparison with JCPDS standard.

Table 1. Crystallographic refined parameters obtained from single crystal data.

Empirical formula	$Li_{0.5}Ce_{0.5}MoO_4$	$Li_{0.5}Ce_{0.25}Pr_{0.25}MoO_4$	$Li_{0.5}Ce_{0.25}Sm_{0.25}MoO_4$
Formula weight	233·5	233·7	236·0
Crystal habit, colour	Black, orange red	Black, orange red	Black, orange red
Crystal size(mm)	0·12 × 0·11 × 0·10	0·16 × 0·11 × 0·08	0·21 × 0·12 × 0·11
Temperature (K)	293(2)	293(2)	293(2)
Radiation	*MoKα*	*MoKα*	*MoKα*
Wavelength (Å)	0·71069	0·71069	0·71069
Crystal system	Tetragonal	Tetragonal	Tetragonal
Space group	$I4_1/a$	$I4_1/a$	$I4_1/a$
a (Å)	5·2943(3)	5·2840(1)	5·2546(3)
c (Å)	11·6254(10)	11·5763(4)	11·5052(11)
Volume/Å^3	325·85(4)	323·22(1)	317·67(4)
Z	4	4	4
Density/g cm^{-3}	4·759	4·802	4·935
F(000)	417·8	418·8	421·8
Scan mode	ω scan	ω scan	ω scan
θmax (°)	32·7	30·5	32·5
$h_{min,max}$, $k_{min,max}$, $l_{min,max}$	(−7, 7), (7, 7), (−17,17)	(−7, 7), (7, 7),(−14, 16)	(−7, 7), (7, 7), (−16, 16)
No. of reflns measured	2669	2507	2630
No. of unique reflns	289	249	277
Absorption correction	Numerical from crystal shape	Multi-scan	Numerical from crystal shape
μ (mm^{-1})	10·656	10·991	11·970
Refinement	F^2	F^2	F^2
R_all, *R_obs*	0·032, 0·026	0·023, 0·025	0·024, 0·018
wR_2_*all*, wR_2_*obs*	0·084, 0·081	0·061, 0·060	0·040, 0·039
GoF	1·227	1·490	1·151
Max/min $\Delta\rho$ e/Å^3	0·511, −1·203	0·781, −0·892	0·459, −0·771

Table 2. Atomic coordinates and occupancies.

Atoms		*x*	*y*	*z*	Occupancy			Wyckoff notation
					LCM	LCPM	LCSM	
Mo		0	0·25	0·125	1	1	1	4*a*
	LCM	0·2409(5)	0·3943(5)	0·0415(3)	1	1	1	16*f*
O	LCPM	0·2411(5)	0·3952(5)	0·0410(2)				
	LCSM	0·255(3)	0·399(2)	−0·0396(2)				
Li		0	0·25	0·625	0·5	0·5	0·5	4*b*
Ce		0	0·25	0·625	0·5	0·25	0·25	4*b*
Pr/Sm		0	0·25	0·625		0·25	0·25	4*b*

RED.[22] The structures were solved by direct method using SHELXL97[23] using the program suite WINGX (version 1·70·01).[24] The molecular packing diagrams were generated using Diamond Version 2·1c.[25] Chemical states of various elements, especially lithium, were deduced using X-ray photoelectron spectra (XPS) (Thermoscientific Multilab 2000 equipment employing Al Kα X-rays). XPS binding energies are accurate within ± 0·1 eV.

2.4 *Ionic conductivity from ac-impedance spectroscopy*

AC impedance measurements were carried out using pelletized samples. Prior to measurement, the pellets were annealed at 700°C for 1 h. Silver paste was applied on both sides of the pellet for better ohmic contact. The coated pellets were heated at 150°C for 1 h to remove the organic component of the Ag-paste. Diameter and thickness of the pellet were approximately 10 mm and 1 mm respectively. The annealed pellets were then placed between two steel electrodes of a home-made conductivity cell (cell constant: LCM = 0·12 cm^{-1}, LCPM = 0·14 cm^{-1}, LCSM = 0·13 cm^{-1}) for ac-impedance measurements (Novocontrol Alpha-A) in the frequency range (1×10^0–3×10^6) Hz (signal amplitude = 0·05 V) from 30 to 700°C at an interval of 50°C. The temperature of samples was equilibrated for 30 min at each temperature point (±1°C, programmable Thermolyne furnace) prior to the impedance measurements. The 50 mV ac-signal voltage was selected after optimisation of parameters related to the sample under test, surface metalic layer coating and electrical circuitry including the impedance analyser. 50 mV was the lowest possible signal amplitude which provided us with good quality reproducible impedance spectra and also allowed us to analyse the spectra for calculation of some useful electrolyte physical constants such as dielectric constant (section 3.3). Polarizability effects at this voltage can be ruled out as repeated ionic conductivity versus temperature runs produced the same conductivity values. Spectra of poor quality were obtained for signal voltages lower than 50 mV.

Table 3. Anisotropic dispalcement parameters ($Å^2$).

Compounds	Atoms	U11	U22	U33	U23	U13	U12
LCM	Mo	0·0093(3)	0·0093(3)	0·0156(4)	0·0000	0·0000	0·0000
	O1	0·0192(13)	0·0128(12)	0·0193(11)	0·0004(11)	0·0050(10)	−0·0033(10)
	Ce/Li1	0·0074(3)	0·0074(3)	0·0074(4)	0·0000	0·0000	0·0000
LCPM	Mo	0·0105(3)	0·0105(3)	0·0155(4)	0·0000	0·0000	0·0000
	O1	0·0195(12)	0·0151(12)	0·0197(11)	0·0003(10)	0·0050(10)	−0·0016(9)
	Ce/Pr/Li1	0·0087(3)	0·0087(3)	0·0082(4)	0·0000	0.0000	0·0000
LCSM	Mo	0·0098(2)	0·0098(2)	0·0146(3)	0·0000	0·0000	0·0000
	O1	0·0196(10)	0·0128(10)	0·0179(9)	-0·0007(9)	0·0032(9)	0·0025(8)
	Ce/Sm/Li1	0·0079(2)	0·0079(2)	0·0079(2)	0·0000	0·0000	0·0000

Table 4. Bond distances and bond angle for $Li_{0·5}Ce_{0·5-x}Ln_xMoO_4$ (x = 0 and 0·25, Ln = Pr, Sm).

Bond distances (Å)			
	LMC	LMCP	LMCS
Mo1−O1	1·776(3) × 4	1.777(3) × 4	1·773(2) × 4
Ln/Li−O1	2·492(3) × 4	2·481(3) × 4	2·467(2) × 4
	2·524(3) × 4	2·516(3) × 4	2·492(2) × 4
Bond angles(°)			
O1−Mo1−O1	107·39(9)	107·42(8)	107·20(7)
	113·7(2)	113·66(18)	114·11(15)
O1−Ln/Li −O1	127·10(8)	126·89(8)	126·91(7)
	78·09(13)	78·43(12)	78·40(11)
	151·16(12)	151·45(10)	151·53(9)
	68·34(7)	68·37(6)	68·56(5)
	76·80(10)	76·70(9)	76·45(8)
	73·83(5)	73·76(5)	73·79(5)
	98·51(5)	98·59(4)	98·62(4)
	134·76(13)	134·54(12)	134·45(11)

3. Results and discussion

3.1 *Differential scanning caloriemetry (DSC)*

Figure 1 shows DSC data for LCM, LCPM and LCSM. DSC analysis showed an endothermic peak at 510°C (±2°C) and two small peaks around 100°C and 150°C (figure 1a). The peaks at around 100°C and 150°C are due to adsorbed water. In order to detect the presence of adsorbed water in LCM and substituted compounds, all compounds were heated for 12h at 120°C under vacuum and DSC was performed under the same condition as the unheated samples. Preheated samples did not exhibit the peaks at 100°C and 150°C. Apart from the endothermic peak at 510°C no other peaks were seen in the DSC analysis of the preheated samples. Therefore, we conclude that peaks observed in the range of 100–150°C for the unheated samples were due to adsorbed water (figure 1b). It is of interest to note that the endothermic peak at 510°C does not show a sharp feature, instead shows a complex behaviour. This feature needs careful investigation to arrive at possible phase transitions in correlation with high temperature XRD studies which are planned in our future study.

3.2 *Crystal structure determination*

Powder diffraction data of LCM, LCPM and LCSM confirmed the formation of single scheelite type phase (JCPDS standard 00-050-0350)[26] $Li_{0·5}Ce_{0·5-x}Ln_xMoO_4$ (x = 0 and 0.25, Ln = Pr, Sm) (figure 2). The single crystal data suggest that all three compounds belong to the space group $I4_1/a$. The details of the structure refinement are listed in table 1. Table 2 gives the coordinates of the atoms, table 3 their corresponding anisotropic displacement parameters and table 4 lists selected bond lengths and bond angles. The position of Ce/Li and Mo were obtained by direct methods. The oxygen was located from the subsequent difference Fourier synthesis. Mo occupies the 4*a* (symmetry: $\bar{4}$) Wyckoff position and the oxygen atom occupies the general Wyckoff site 16*f*. Li and Ce share the same Wyckoff site 4*b* (symmetry: $\bar{4}$) where Li and Ce, respectively, occupy half of the 4*b* site (table 2). The occupancies of Li and Ce were taken according to their stoichiometry during the least square refinement and the resulting refinement gives a reasonable R factor (table 1). Further, in substituted $Li_{0·5}Ce_{0·5}MoO_4$, the substituent i.e., Pr and Sm occupy the same position as Ce. Therefore, for refinement of LCPM and LCSM, the same approach was used as for LCM for the occupancy assignment. Equivalent anisotropic displacement parameter (EADP) command was used to refine the thermal parameter of Li and Ln (Ln = Ce, Pr, and Sm) simultaneously. The structure consists of MoO_4 tetrahedra and Ce/LiO_8 polyhedra. The Ce/LiO_8 polyhedra

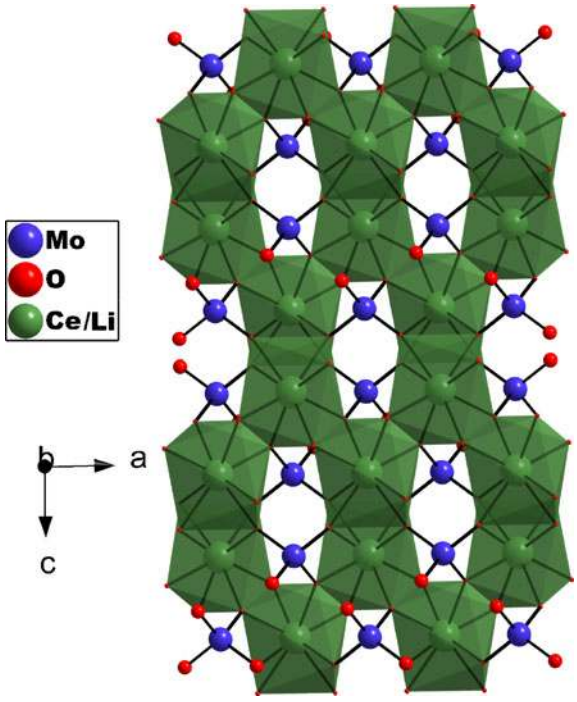

Figure 3. Crystal structure of LCM showing the arrangement of atoms in MoO_4 tetrahedra and Ce/LiO_8 polyhedra.

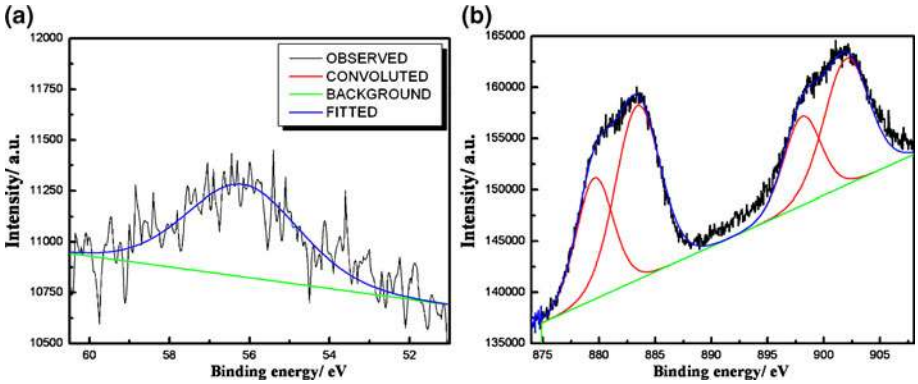

Figure 4. XPS plot for $Li_{0.5}Ce_{0.5}MoO_4$; (**a**) Lithium is in +1 oxidation state, (**b**) Cerium is in +3 oxidation state.

share edge with each other whereas MoO_4 tetrahedra are isolated from each other (figure 3). MoO_4 tetrahedra shares corner with Ce/LiO_8 polyhedra. Ce/Li and Mo ions arrange in respective rows when viewed along either *a*-axis or *b*-axis, while along the *c*-axis Ce/Li and Mo ions are alternately arranged. The cell parameter becomes smaller due to substitution at the Ce site and this is due to the decrease of the ionic radii as one goes across the lanthanides in the periodic table. Therefore, with substitution at the Ce site, the conductivity of the substituted compound is also expected to decrease compared to the parent LCM.

Powder diffraction patterns are not useful to detect the presence of Lithium in these compounds since the scattering factor of Lithium is substantially smaller than the other elements. Spectroscopic techniques like XPS and AAS are generally useful to detect the presence of such elements occurring in small quantities both in the lattice and also as an impurity. The presence of lithium in the LCM compound was detected by XPS. X-ray photoelectron spectroscopy gives a peak at binding energy = 56·78 eV with FWHM = 3·45, corresponding to Li^+ peak (figure 4). AAS, (Perkin Elmer Analyst 200) taking Li_2CO_3 as a standard also confirmed the presence of lithium. Indeed, attempts to synthesize LCM without any Li source does not generate a scheelite phase (figure 5) substantiating that lithium is not present as an impurity but is an integral part in the compound. It is of interest to note that both lithium and cerium occupy the same position although they are chemically different. This feature indeed is observed in some structures reported in literature. As a representative case, in the structure of lanthanum lithium titanate,[7] which focuses on the lithium ion migration, the authors assign the lithium to the lanthanum site because of the ability of the lithium ion to migrate. They also provide an indirect proof by evaluating Sr substitution at the La site. In an earlier report from our own group[27] on the structure of $CeVO_4$, Li substitution was examined at the Ce site in comparison with Fe and Ca ions at the same site. It is obvious that the rigidity of MO_4 might prevent the insertion of Li ions at the B site.

3.3 *Ionic conductivity from ac-impedance spectroscopy*

In general, for all samples, impedance spectrum comprised of a high frequency semicircle and a low frequency spike in the temperature range from 30°C to approximately 400°C as shown for the LCM sample in figures 6(a–c). With an increase in temperature, the semicircle disappeared and only a spike was observed in the Re(Z′)–Im(Z″) plots (Z: impedance) (figure 6d). The high frequency semicircle analysed using a

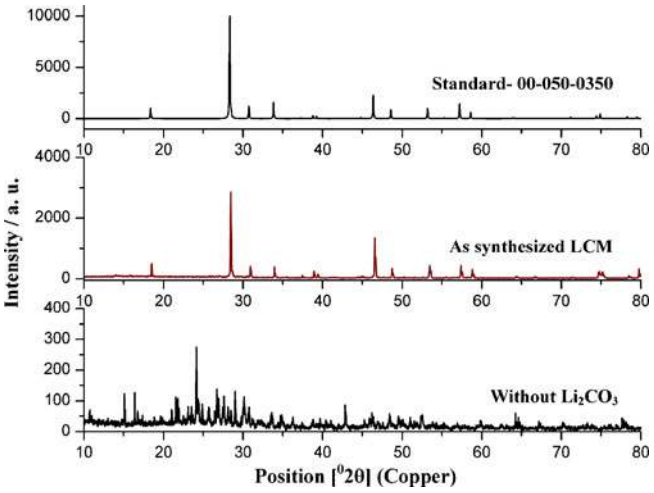

Figure 5. Comparison of powder patterns of (unheated) LCM with standard pattern and without Li_2CO_3.

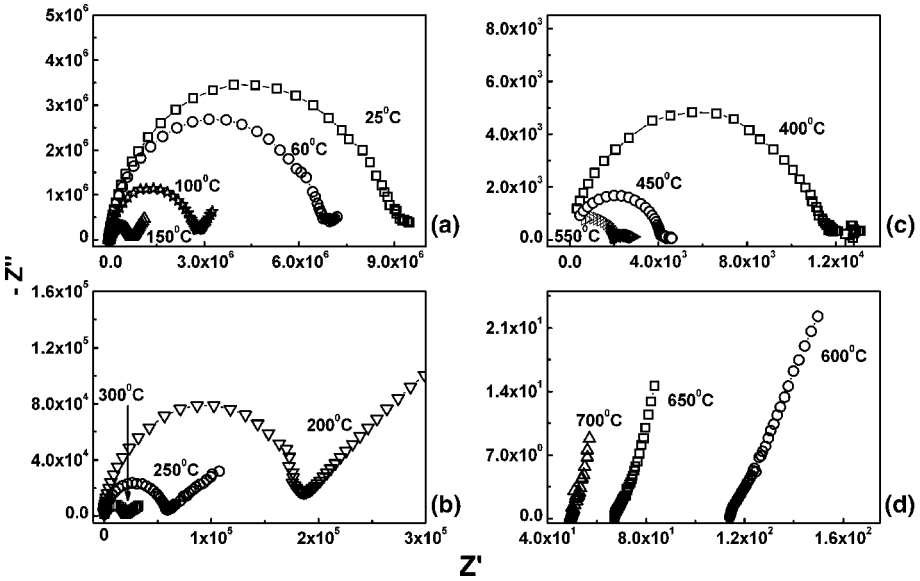

Figure 6. ac-impedance spectra for preheated LCM in various temperature regimes (conductivity cell configuration: Ag| Electrolyte |Ag, Ag = Silver, (1×10^0–3×10^6) Hz; ac signal voltage amplitude = 0.05 V).

resistor and constant phase element (Q) in parallel (ZView V2.6b, Scribner Associates) resulted in a dielectric constant estimate of approximately 70–80. This is slightly higher than the value of approximately 35 reported for scheelite molybdates.[28] The higher estimate of the dielectric constant is attributed to stray capacitance effects which may arise due to poor contact, roughness at the electrode and electrolyte interface. However, this does not affect the estimate of effective sample resistance obtained from the intersection of the low frequency spike with real axis Re (Z′) of the impedance for all samples and temperature regimes. Figure 7(a) shows the ionic conductivity as a function of temperature (ranges 30–700°C) for unheated LCM, LCPM and LCSM. Initially the ionic conductivity of LCM decreases to $9{\cdot}3\times10^{-8}$ Ω^{-1}cm^{-1} till 100°C ($\sigma_{25°C} = 9{\cdot}6\times10^{-7}$ Ω^{-1} cm^{-1}) and then starts to increase with temperature (the errors estimated to be in the range of 10–15%). At 700°C the conductivity for all the samples reaches a value of approximately 8×10^{-4} Ω^{-1}cm^{-1}. For the substituted LCM compounds viz., LCPM and LCSM, the room temperature ionic conductivities are lower than the unsubstituted LCM and this trend is observed nearly over the entire temperature range. So the conductivity follows the trend: LCM>LCPM> LCSM. These observations can be explained on the basis of change in the unit cell volume of the compounds (c/f table 1). As we go from Ce to Pr to Sm the ionic radius decreases. As a result the volume also decreases. The non-trivial behaviour in ionic conductivity as a function of temperature of the unheated samples is attributed to adsorbed moisture and was confirmed by DSC measurements (figure 1). Further, in order to determine the effect of adsorbed moisture on ionic conductivity, LCM (LCPM and LCSM) pellets were heated at 120°C under vacuum for 12 h. The measured conductivity versus temperature of these samples (hereafter referred to as preheated samples) is shown in figure 7(b). The conductivity at 25°C for LCM is $1{\cdot}3\times10^{-8}$ Ω^{-1}cm^{-1}, which is lower by nearly two orders of magnitude compared to the unheated LCM. Similar lowering in ionic conductivity was also observed for LCPM ($\sigma_{25°C} = 1\times10^{-9}$ Ω^{-1}cm^{-1}) and LCSM ($\sigma_{25°C} = 1{\cdot}8\times10^{-10}$ Ω^{-1}cm^{-1}). No decrease in ionic conductivity with increase in temperature (up to 100°C) is observed in these samples. The conductivity increased gradually with increase in temperature reaching a high value of approximately $2{\cdot}5\times10^{-3}$ Ω^{-1}cm^{-1} at 700°C (LCPM: $\sigma = 1{\cdot}3\times10^{-3}$ Ω^{-1}cm^{-1}; LCSM: $\sigma = 8.9\times10^{-4}$ Ω^{-1}cm^{-1}). Similar to preheated LCM, the preheated LCPM and LCSM also did not exhibit any minima in the conductivity versus temperature trace. The lowering in ambient temperature ionic conductivity values and disappearance of the minima at approximately 100°C strongly suggests presence of adsorbed water in the as-synthesized (unheated) samples.

With substitution, the cell volume decreases resulting steric effects to lithium ion migration. This is also

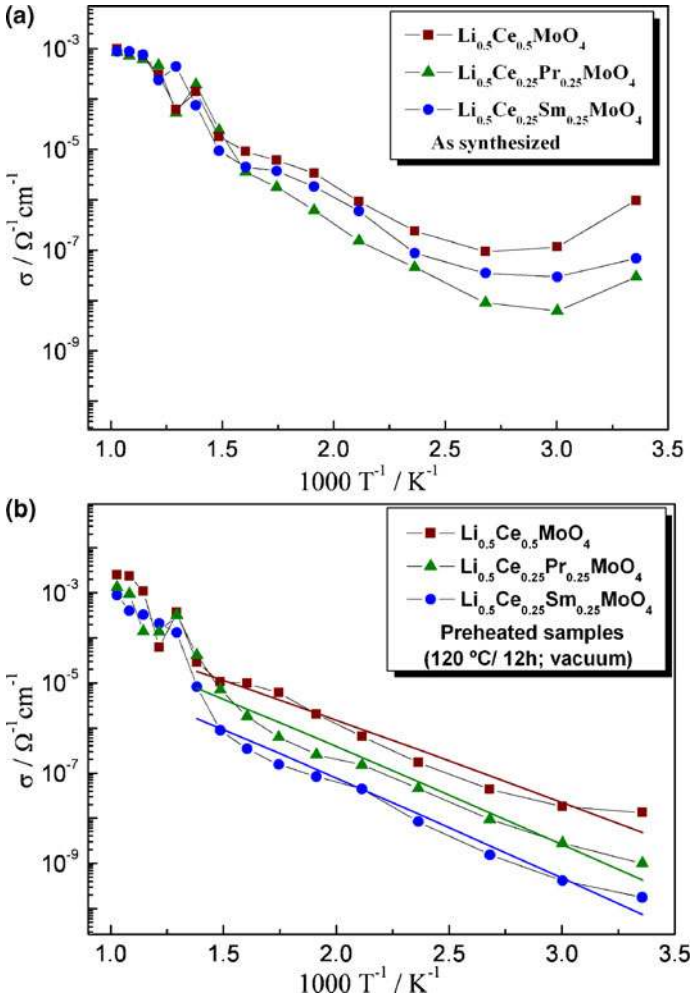

Figure 7. Ionic conductivity from ac-impedance spectroscopy for $Li_{0·5}Ce_{0·5-x}Ln_xMoO_4$ (x = 0 and 0·25, Ln = Pr, Sm). (**a**) as synthesized sample, (**b**) preheated samples (120°C/ 12 h; vacuum) (conductivity cell configuration: Ag| Electrolyte |Ag, Ag = Silver, (cell constant: LCM = 0·12 cm^{-1}, LCPM = 0·14 cm^{-1}, LCSM = 0·13 cm^{-1}).

evident from the activation energy (E_a) (in the temperature range of 25–450°C) estimates from figure 7 (b). While for LCM, E_a = 0·4 eV, for LCPM and LCSM $E_a \approx$ 0·5 eV (due to adsorbed water, no clear trend in E_a was observed for the unheated samples. While for LCM, E_a = 0·36 eV, for LCPM and LCSM $E_a \approx$ 0·56 eV and 0·4 eV, respectively). An interesting observation is the anomalous variation in ionic conductivity observed at approximately 500°C (figure 6b). The anomaly in the ionic conductivity can be attributed to the phase transition which occurs at 510°C (±2°C) for each sample. The phase transition appears to be reversible as the powder pattern remains the same when the samples were brought back to room temperature. This is also observed in case of the LCPM and LCSM samples.

4. Conclusions

In this study, we have demonstrated lithium ion conductivity in $Li_{0·5}Ce_{0·5-x}Ln_xMoO_4$ (x = 0 and 0·25, Ln = Pr, Sm), a solid electrolyte with a scheelite type structure established by single crystal diffraction studies. The scheelite structure of $Li_{0·5}Ce_{0·5}MoO_4$ is favourable for sustaining high values of ionic conductivity in a wide temperature range, especially in the temperature regime of 300–700°C. The presence of adsorbed moisture and its influence on the conductivity

behaviour point out to the precautions to be taken while making devices. The ionic conductivity following a phase transition at approximately 510°C is higher compared to the corresponding normal structure. While substitution at the cerium site with other lanthanides (LCSM and LCPM) resulted in stable compounds with the same scheelite structure, the ionic conductivity was lower than the parent LCM. Interestingly, the ionic conductivity of the substituted compounds is not appreciably low in the temperature range of ~400–700°C. Due to existence of several possibilities for synthesis of LCM compounds in various morphologies such as thin films, we presume that they will also be beneficial for applications in miniaturized lithium battery technologies (e.g., micro-batteries) for operation over a wide range of temperatures.

Acknowledgements

The authors thank Mr. I S Jarali for DSC and AAS measurements and Ms. Supti Das for conductivity measurements. TNG thanks the Department of Science and Technology (DST) for funding. We also thank funding under DST-FIST (Level II) for single crystal facility and Indian Institute of Science (IISc) for XPS facility.

References

1. Minami T, Tatsumisago M, Wakihara M, Iwakura C, Kohjiya S and Tanaka I 2005 *Solid state ionics for batteries*, Springer
2. Tarascon J M and Armand M 2001 *Nature* **414** 359
3. Aono H, Imanaka H and Adachi G Y 1994 *Acc. Chem. Res.* **27** 265
4. Knauth P 2009 *Solid State Ionics* **180** 911
5. Belous A G, Novitskaya G N and Polyanetskaya S V and Gornikov Yu I 1987 *Izv. Akad. Nauk SSSR* **23** 470
6. Inaguma Y, Chen L Q, Itoh M, Nakamura T, Uchida T, Ikuta H and Wakihara M 1993 *Solid State Commun.* **86 (10)** 689
7. Inaguma Y, Chen L Q, Itoh M and Nakamura T 1994 *Solid State Ionics* **70** 196
8. Adachi G Y, Imanaka N, Aono H 1996 *Adv. Mater.* **8** 127
9. Stramare S, Thangadurai V and Weppner W 2003 *Chem. Mater.* **15** 3974
10. Aono H, Sugimoto E, Sadaoka Y, Imanaka N and Adachi G Y 1991 *Solid State Ionics* **47** 257
11. Bruce P G and West A R 1983 *J. Electrochem. Soc.* **130 (3)** 662
12. Kanno R, Hata T, Kawamoto Y and Irie M 2000 *Solid State Ionics* **130** 97
13. Murayama M, Kanno R, Irie M, Ito S, Hata T, Sonoyama N and Kawamoto Y 2002 *J. Solid State Chem.* **168** 140
14. Thangadurai V and Weppner W 2005 *J. Am. Ceram. Soc.* **88** 411
15. Thangadurai V and Weppner W 2005 *Adv. Funct. Mater.* **15** 107
16. Murugan R, Thangadurai V and Weppner W 2007 *Angew. Chem. Int. Ed.* **46** 7778
17. Robertson A D, West A R and Rithie A G 1997 *State Ionics* **104** 1
18. Egorova A N, Maier A A, Nevskii N N and Provotorov M B 1982 *Neorganicheskie Materialy* **18(12)** 2036
19. Odaki T, Hashimoto K and Toda Y 2008 *J. Jpn. Soc. Colour Mater.* **81(3)** 73
20. Klevtsov P V, Protasova V I, Kharchanko L Yu and Klevtsova R F 1973 *Sov. Phys.-Cryst.* **18** 523
21. SMART (V 5.628), SAINT (V 6.45a), Sadbs, XPREP, SHELXTL; Bruker AXS Inc.; Madison, WI, 2004
22. Oxford Diffraction 2009. CrysAlis CCD, CrysAlisPro RED. Version 1.171.33.34d, Oxford Diffraction Ltd., Abingdon, Oxfordshire, England
23. Sheldrick G M 2008 *Acta Crystallogr.* **A64** 112
24. Farrugia L J WinGX (V 1.70.01) 1999 *J. Appl. Crystallogr.* **32** 837
25. Brandenburg K, DIAMOND. Version. 2.1c., Crystal Impact GbR, Bonn, Germany, 1999
26. Egorova A N, Provotorov M B and Maier A A 1981 *Neorganicheskie Materialy* **17(6)** 1130
27. Mahapatra S, Vinu R, Saha D, Row T N G and Madras G 2009 *Applied Catalysis A: General* **361(1-2)** 32
28. Brower W S Jr and Fang P H 1969 *J. Appl. Phys.* **40(12)** 4988